Coevolving edge rounding and shape of glacial erratics; the case of Shap granite, UK

Paul A. Carling[1]

[1]School of Geography & Environmental Science, University of Southampton, Southampton, SO17 1BJ, UK

Correspondence to: Paul A. Carling (p.a.carling@soton.ac.uk)

Abstract

The size distributions and the shapes of detrital rock clasts can shed light on the environmental history of the clast assemblages and the processes responsible for clast comminution. For example, mechanical fracture due to the stresses imposed on a basal rock surface by a body of flowing glacial ice releases initial 'parent' shapes of large blocks of rock from outcrop, which then are modified by the mechanics of abrasion and fracture during subglacial transport. The latter processes produce subsequent generations of shapes, possibly distinct in form from the parent blocks. Lacking is a complete understanding of both the processes responsible for block shape changes and the trends in shape adjustment with time and distance away from the source outcrop. Field data on edge rounding and shape changes of Shap granite blocks (dispersed by Devensian ice eastwards from outcrop) are used herein to explore the systematic changes in block form with distance from the outcrop.

The degree of edge rounding for individual blocks increases in a punctuated fashion with the distance from the outcrop as blocks fracture repeatedly to introduce new fresh unrounded edges. In contrast, block shape is conservative, with parent blocks fracturing to produce self-similar 'child' shapes with distance. Measured block shapes evolve in accord with two well-known models for block fracture mechanics — 1) stochastic and 2) silver ratio models — towards one or other of these two attractor states. Progressive reduction in block size, in accord with fracture mechanics, reflects the fact that most blocks were transported at the sole of the ice mass and were subject to the compressive and tensile forces of the ice acting on the stoss surfaces of blocks lying against a bedrock or till surface. The interpretations might apply to a range of homogeneous hard rock lithologies.

Short Summary

Edge rounding in Shap granite glacial transported boulders is an irregular function of distance from the source outcrop in northern England, UK. Block shape is conservative, evolving according to block fracture mechanics — stochastic and silver ratio models — towards either of two attractor states. Progressive reduction in size occurs to blocks transported at the sole of the ice mass where the blocks are subject to the compressive and tensile forces of the ice acting against a bedrock or till surface.

Key words

Glacial erratics, erratic rounding, erratic shape, fracture, subglacial

1 Introduction

The concentration, size, shape, and the degree of rounding of glacial ice-transported blocks of rock may change with distance from the source outcrop. Spatial trends in concentration have been used frequently to indicate preferred ice flow directions (Kujansuu & Saarnisto, 1990; Evans, 2007, Benn & Evans, 2011, p. 675). Concentrated bands of ice-freighted erratics are referred to as 'indicator plumes', 'indicator trains' or 'indicator fans', with concentrations dropping off rapidly outside of the plumes due to ice-flow induced dispersion (Larson & Mooers, 2004). None-the-less, concentration is also sustained by comminution, whereby blocks fracture, or abrade to form smaller blocks and fragments through time and distance from the source outcrop. In contrast to dispersion, there has been less focus on changes in size, shape, and edge-rounding with distance from source (Benn & Evans, 2011). The changes in the shape of blocks are functions of the mechanical properties of the blocks, primarily rock strength and structure, as well as the physical processes promoting comminution. A change in block shape also represents a change in block size. To explore the controls on edge rounding and the shape of erratics, dispersal from a well-known exposure of the Shap granite (Sg) in the UK was examined in the present study. Improved understanding of process controls related to edge rounding and fracture should shed light on the associated basal ice dynamics related to block form changes generally. The two key issues are: 1) the relative importance of fracture mechanics in reducing block size in contrast to edge-rounding and 2) whether edge-rounding and shape coevolve with distance from the source outcrop.

1.1 The Study Area and Context of the Study

The exposure of the Sg pluton occupies a small area (*c*., 7 km^2) in the eastern English Lake District (Fig. 1) defining a distinct, small, source area for granite blocks. The variation in the concentrations of Sg blocks with distance from the pluton has been used as a key indicator of the directions of ice

movement across northern England (reviewed by Carling *et al*., 2013) during the Dimlington Stadial (*c*., 30 ka BP to 14.7 ka BP) within the overall period of the Devensian glaciation (*c*., 33 ka BP to 11.7 ka BP). Around the Late Glacial Maximum (LGM: 26.5 ka BP to 19 ka BP, Clark *et al*., 2009), the region was covered by ice, several hundred metres thick (Evans *et al*., 2009), and Sg blocks were entrained from the subglacial bedrock (Ugelgiv *et al*., 2016). Long Fell, on the eastern margin of the exposed pluton, is a kilometre-scale rôche moutonnée, severely ice-plucked in the east and south-east at Wasdale Crag (Fig. 1), with smooth, ice-planed surfaces occurring to the north, west and on the summit (point 452m), indicating the erosional effects of moving ice and debris (Hallet, 1981). The west to east change in the style of erosion, from smoothing to plucking, is consistent with ice in the vicinity of the pluton moving predominately to the east in an early phase (*c*., 29-25 ka BP; Livingstone *et al*., 2012; Merritt *et al*., 2019) of the Dimlington Stadial, and generally northwards across the pluton subsequent to 22 ka BP, *i.e.* towards the end of the LGM (Livingstone *et al*., 2012; Merritt *et al*., 2019); the latter supposition consistent with the W.S.W. to E.N.E. orientation of glacial striations on the pluton (Nicholson, 1868).

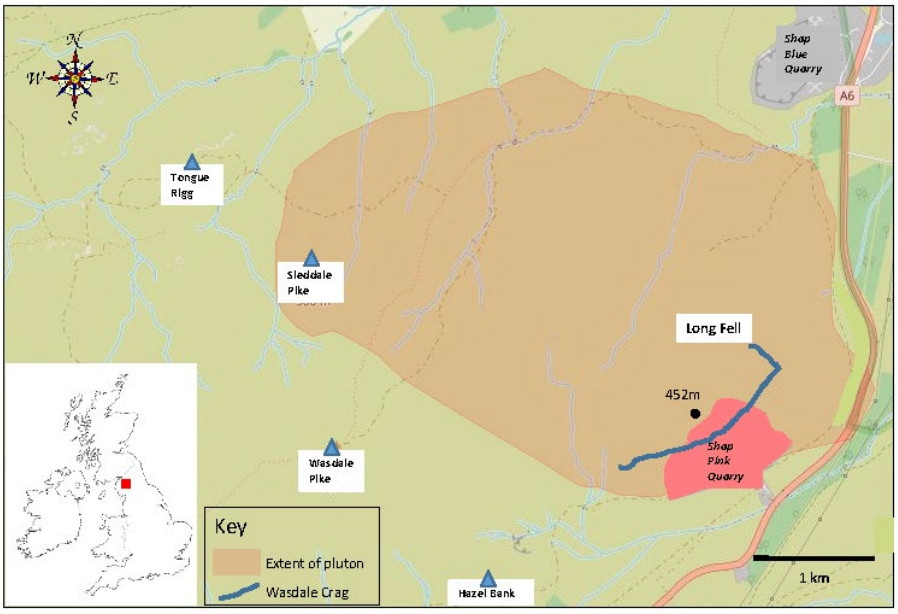

Figure 1: Location of the Shap granite pluton. The central portion of the ice-plucked outcrop (Wasdale Crag) crag has been destroyed by quarrying. Base map is from CC BY © OS Map Local data.

Approximate extent of the Shap Granite pluton outcrop from the British Geological Survey (https://www.bgs.ac.uk/map-viewers/geoindex-onshore/).

In terms of concentration, the dominant dispersal of Sg erratics, during the early phase of the Dimlington Stadial (Stage I; 29-25 ka BP; Merritt *et al*., 2019) was eastward (Carling *et al*., 2013) within sustained ice flow through the topographically controlled corridor of the Stainmore gap across the north Pennines hills (Fig. 2A). The plume extended as far as the east coast of England; a distance more than 100km (Fig. 3). Block size tends to diminish with distance, although examples of far-travelled large blocks occur sparingly (Carling *et al*., 2023). Due to shifting ice divides and competing ice dispersal centres (Merritt *et al*., 2019), subsequently two Sg plumes dispersed in southerly directions until, in the late stadial, erratics briefly were dispersed northwards from the vicinity of the pluton (Carling *et al*., 2013) in accord with the ice movements reported by Livingstone *et al*. (2012). These latter dispersal directions are not considered further herein. The focus solely is on those erratics the final transport vectors (direction and distance) which are roughly due east, defining a simple linear direction over which changes in the nature of the erratic populations might be measured.

Less well understood than directions of travel and changes in concentration, is the process of edge-rounding and shape changes of Sg blocks that accompany size reduction. The granite is an ideal choice for study as the composition and texture is uniform (Grantham, 1928), mostly giving a massive, unlayered, structure to individual blocks. Layering, such as found within sedimentary rocks, would add complexity to the study of shape evolution, which is avoided in this study. Hopkins (1849) had commented briefly on the rounding of Sg blocks (density ~ 2.61 tonnes m^{-3}) as size reduces towards the east coast, yet such rapid changes in form are seemingly at odds with the high strength of the rock. The strength of Sg in compression exceeds 207 MPa (Holland, 1959;

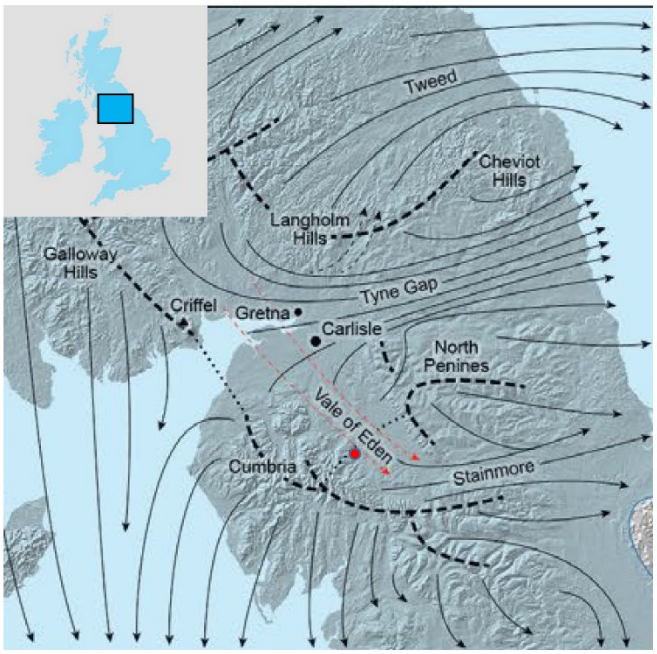

Figure 2: Reconstructed of Stage I (29-25 ka BP) of the last British-Irish Ice Sheet around the Solway Firth (from Merritt et al., 2019. Reproduced with permission) in northern England Stage (inset panel). Eastward ice flow through prominent topographic corridors occurs across the north Pennines. Broken and dotted lines refer to ice divides. Arrows indicate ice-flow vectors (dotted arrows indicate alternative ice-flow scenarios). Topography from NEXTMap digital elevation data. Shap granite erratic plume dispersed to the east from the pluton (red dot) chiefly over Stainmore (see Fig 3).

Day & Goudie, 1977; Goudie, 2006) such that the rock is considered 'very strong' (British Standards, 1981). Despite the rock strength, Hodgson (1870) had remarked on how seemingly rapid rounding of granite might be aided by rock friability due to a high mica content associated primarily with biotite (Firman, 1953). Biotite is soft compared with the large phenocrysts of feldspars and quartz (Firman, 1953) that dominate the granite composition. Nevertheless, there has been no investigation of the changes in shape and rounding of Sg blocks with distance from the source; with very few granite blocks visually maintaining significant mass over 10's of km. A study of blocks exposed on the modern land surface, away from major watercourses, should reveal rock-wear processes associated with glacial transport as there has been negligible losses to Sg surfaces due to post-glacial subaerial weathering (Wager, 1944; Parsons & Lee, 2005). The few weathered examples of blocks exhibit phenocrysts standing proud (3-5mm) of the matrix, as the mica is readily subject to chemical weathering if *buried*

but the feldspars are not much altered (Wager, 1944). Consequently, an hypothesis was proposed: '*Sg ice-transported blocks would display systematic changes in edge-rounding and shape'*; with an aim *'to demonstrate if edge rounding and shape coevolve with distance to the east from the pluton'.*

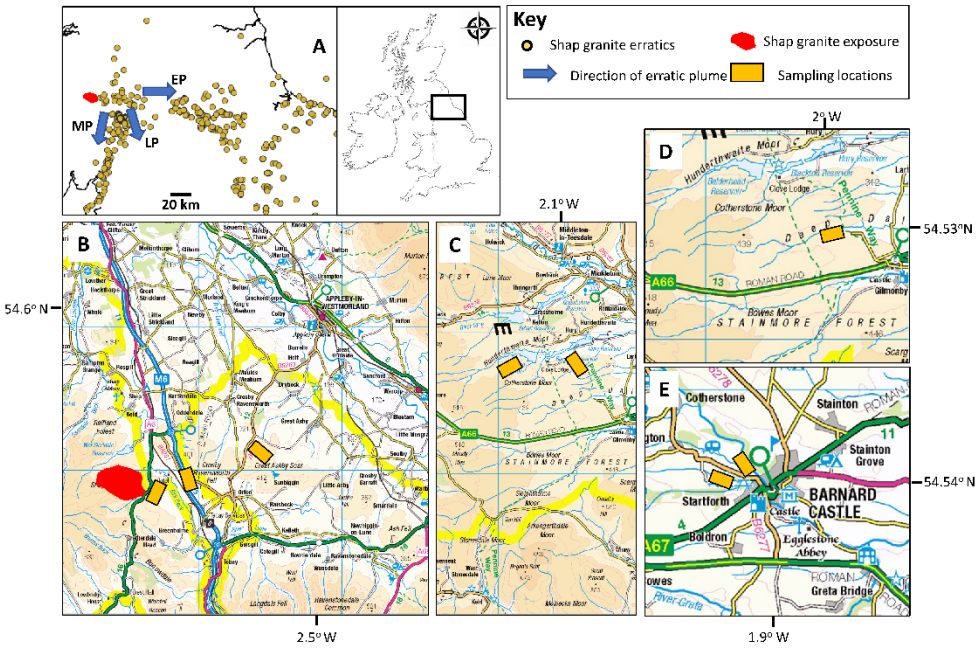

Figure 3: A) Spatial distribution of examples of Shap granite erratics within the study area, northern England (inset), showing the early easterly-directed plume (EP) and the later southerly Mint and Lune plumes (MP & LP) relative to the source outcrop of Shap granite. Sampling locations shown are indicative of the general sampling areas: B) Wasdale Bridge, Haybanks, Blasterfield C) upper Teesdale; D) Levy Pool; E) Barnard Castle. See main text for details. Base maps based on CC BY © OS 1:250 000 Scale Colour Raster™.

Shape (and size) changes in a Shap granite block occur due to three predominant processes which scale from effecting small areas of a block to larger areas:

1) abrasion, whereby grain-size fragments (*e.g.,* phenocrysts) are ground-off the block surface (Haldorsen, 1981; Benn & Evans, 2011) primarily by shear stresses associated with blocks moving across a bedrock or till surface in the direction of basal ice motion, or by ice and till moving over stationary blocks lodged against the substratum - this process can result in distinct rounded surfaces on a block (Boulton, 1978; Hallet, 1979);

2) spallation, whereby flakes of rock are freed from the surface of the block (Olsen, 1983) due to externally-derived and internally-derived tensile deviatoric stresses in the rock, both imposed by the motion of the ice overburden, with the shear stresses acting on planes at less than the block scale (Li *et al*., 2018) – this process reduces block mass but results in localized scarred surfaces;

3) fracture (Buscarnera & Einav, 2021) whereby the 'parent' block splits into substantial parts (often two; here referred to as 'child' products). The propagating fissure ultimately may be due to compression loading but, at the block surface, it is the result of a tensile stress (acting on a plane at block scale) flexing the stoss surface of a brittle block lying on a hard basal surface, leading to fissure development often transverse to the direction of basal ice motion (Morland & Boulton, 1975; Hallet, 1996; Benn & Evans, 2011, p264). The tensile strength of a rock is typically an order of magnitude less than the compressive strength (Li *et al*., 2018). This tripartite classification informed the Method.

To address the hypothesis, the focus of the study is abrasion and fracture, but observations on spallation were obtained for completeness, with the latter results reported within Supplementary Information. There is justification from studies of bedrock outcrop erosion by basal ice that both the degree of abrasion of bedrock surfaces and the number of fracture events are related to time in transport (Cohen *et al*., 2006) and thus the distance erratics are moved.

2 Method

Shap granite blocks were sampled along a west to east transect, starting from below Wasdale Crag. It was assumed that all the sampled blocks were from the same population subject to basal traction transport (*vis*. Boulton, 1978) for much of the transport histories; the population being a coarser

component of a subglacial traction till(*sensu* Evans *et al*., 2006) deposited during the waning phase of the easterly phase of ice motion (Fig. 3A) (Hallet, 1979). Blocks (*L* > *c*., 1.0 m) were located by field walking. Locations sampled include Wasdale Old Bridge, Haybanks, Blasterfield, sites near Barnard Castle in Teesdale and Levy Pool near Brough (Table S1), respectively 0.8 km, 3.5 km, 8.4 km, *c*., 36 km and *c*., 41 km from the Wasdale Crag outcrop (Fig. 3). The sites selected were known to have sufficient erratics within defined areas for sampling. However, to obtain similar sample sizes, the areas searched for the final two locations necessarily increased as the surface density of blocks decreased eastwards. Examples of erratics were selected that were sitting on exposed bedrock or till surfaces, so as not to be partially buried. Distance from the source outcrop is assumed to relate to time in transport.

At each location, edge, and shape measurements and scar enumeration were made on thirty blocks as briefly described below; the full procedure developed within Supplementary Information. The sample size was found to be sufficient (Daniel, 1999; Conroy, 2018) for the aims of the project and, moreover, interpretation of data trends became possible once the sample size *n* > 30 at each location. These data were supplemented by a regional shape data compendium (Carling *et al*., 2013). Changes in block size with distance from the pluton are not considered herein using field data, as a statistically significant sample size at each location would have to be prohibitively large to reflect the complete size range of blocks. Rather block size changes are considered within a theoretical framework related to shape changes. Blocks are considered as cuboids consisting of *faces* and *edges*.

In accord with 1) abrasion: edge rounding was measured after Wentworth (1923; Kirkbride, 1985). In brief, each of the three most tightly rounded edges on the visible portion of each block was defined by a chord (l), delimiting a segment of the block beneath each rounded edge, to give between 80 and 90 values for each location. Consideration of the height (h) of the segment in relation to the chord length constrains the radius (r_c) of an inscribed circle beneath the rounded edge, which radius is a measure of the degree of rounding:

$$r_c = \frac{l^2}{8h} + \frac{h}{2} \quad (1)$$

The radius of curvature reduces as the chord length reduces towards zero and often a right-angle corner occurs when r_c approaches 0. More rounded blocks have larger radii of curvature than less rounded blocks as the sizes of the inscribed circles increase as edges become less sharp. In similar fashion, the edge rounding was measured for joints bounding *in situ* Shap granite blocks constituting the outcrop of Wasdale Crag. These latter data provide a base line of the degree of edge rounding of blocks which have been subject to ice abrasion in place, but without subsequent transport.

To consider 3) shape changes by fracture: from initial field reconnaissance, blocks close to the source often appear cubic, but polyhedrons occur sparingly - ranging from wedges to prismatoids. Further from the source more ellipsoidal forms are evident. Consequently, to obtain an indication of the shape of a cuboid or an ellipsoid block, the lengths of the three orthogonal axes: long axis (*L*); medium axis (*M*) and the short axis (*S*) were recorded in the field – polyhedrons were not sampled – to give *c*., 30 values for each location. Consideration of the mechanics of shape changes also sheds light on the size reduction process with distance. Fracture within individual blocks is sometimes associated with joints and other block-scale planes of weakness. Yet, ice compressive force is the predominant mechanism for significant progressive change in shape for homogeneous granite blocks, inducing tensile fracture and block size reduction. Shape and size changes were examined either via a stochastic fracture model, applicable to fracture at right-angles to either of the *L*, *M* or *S* axes (Domokos *et al*., 2015) of ellipsoidal blocks or, in accord with the silver ratio model applicable to cuboid blocks fracturing across the *M*-axis alone (Buscarnera & Einav, 2021), as is explained in the Results.

3 Results

3.1 Edge rounding

As is evident from the form of equation 1, rounding is a positive function of the square of the length of the chord of the segment, l, and an inverse function of the segment height, h (Fig. 4). As the inscribed radius values are obtained from both the values of l and h (Equation 1), there is an element of co-variance between the two axes in both panels A and B of Fig. 4. However, plotting the data in this manner allows ready visualization of the trends of the radius data (r_c) relative to the variation in the controlling parameters (l,h). Lower limits to data plotting positions occur in both panels equal to: $r_c = l/2$ and $r_c = h$ respectively.

The joint rounding on the pluton is less developed in comparison with the rounding of edges of blocks only 0.8km away at Wasdale Old Bridge (Fig. 4). Although the range in heights of the segments are similar for both locations, the range in chord lengths for the pluton includes smaller values giving overall 'sharper' average edge profiles for the pluton joints in contrast to the Wasdale Old Bridge blocks. It is evident that any 'parent' blocks newly entrained from the outcrop will exhibit both lightly rounded joint edges (glacially abraded when *in situ*) as well as sharp, fresh edges, the latter due to fracture upon release from the outcrop. However, although the initial lightly rounded edges can be further rounded with distance, fracture of entrained blocks introduces new 'sharp' edges as detailed next.

Although as distance increases larger radii are more frequent, small radii also occur at distance (Fig. 4). It is unlikely that small radii can survive abrasive transport over several 10's of km from the pluton, rather repeated fracture introduces new sharp edges and thus new small radii to different generations of blocks. These new sharp edges begin to round far from the pluton. Although the plots of Fig. 4 are developed considering singular data points from many blocks, if the trends are considered to represent the rounding evolution that would occur for individual blocks, then the black arrows indicate the general direction of edge rounding evolution (*i.e.,* Fig. 4 panel A: if *h* is constant and *l* is variable; panel B: if *l* is constant and *h* is variable). The linear functions in Fig. 4B allow ready comparison between locations such that, for any value of *h*, the degree of edge rounding is more pronounced with

distance from the pluton; specifically, the linear curves (green, blue, purple, and red) have increasing values of the constant (*i.e.*, 1.71, 4.37, 4.69; 5.53 respectively). Similar linear functions for values of *l* can be applied to Fig. 4A but, for the sake of clarity, these curves are not plotted. The detail of edge

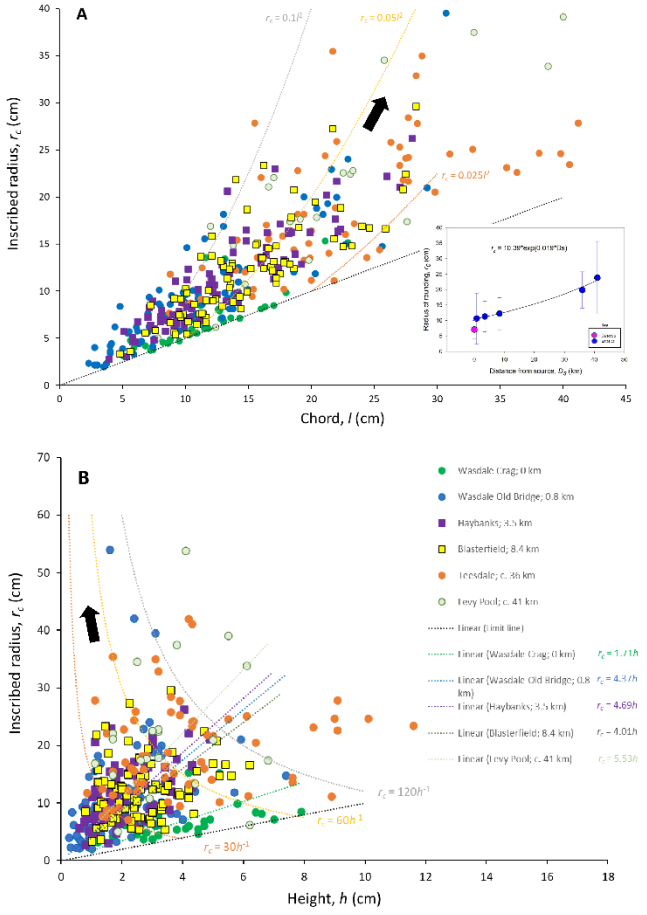

Figure 4: Trends in the values of the inscribed radius as a function of: A) chord length, and; B) segment height. Black arrows indicate the direction of travel of the hypothetical function for an individual block (see main text). Examples of hypothetical curves (brown, yellow and grey) for the trends in individual clast evolution are given for both $r_c \propto l^2$ *and* $r_c \propto h^{-1}$*. Key in panel B also applies to panel A. Inset panel shows mean and s.d. of edge rounding as function of distance from outcrop.*

rounding is considered within the Discussion, as edge-rounding of individual blocks is not a smooth function of distance from the source as might be inferred from the black arrows in Fig. 4 and from the inset figure of mean edge rounding with distance from the outcrop (Fig. 4 inset panel). The latter figure depicts an exponential increase in the mean radius of curvature with distance (D_s) from the source outcrop:

$$r_c = 10.3881e^{(0.0194D_s)}. \quad (2)$$

3.2 Shape evolution

In the context of natural hexahedrons, the *stochastic model* of progressive fracture due to the stress of compression (Domokos *et al*., 2015), describes the generation of ellipsoids with the orthogonal axes length proportions: 2.32; 1.52: 1 (Fig. 5A), whereas the *silver ratio* progressive fracture model (Buscarnera & Einav, 2021) describes the generation of cuboids with the edge length proportions: $\sqrt[3]{2^2}$; $\sqrt[3]{2}$; 1, *i.e*.; 1.59: 1.26: 1 (Fig. 6A). In the former model, a fracture plane is orthogonal to any of the three sides of a cuboid (enclosing the ellipsoid) and separates two pieces of equal mass. In the silver ratio model, a fracture plane occurs orthogonal to the current longest axis, separating two pieces of equal mass. In nature, deviation from these two models can occur such that shape self-similarity, in terms of axial ratios, is not maintained necessarily upon successive fracture events if the subsequent fracture is across an axis that differs from the previous fracture event. Fracture across the plane of the short axis was observed in nature (Fig. 5B). However, systematic fracture across the plane of the long axis (Fig. 5C) and across the medium axis (Fig. 5D; Fig. 6B) appeared predominant (*vis* Benn, 1992) for the blocks observed in the field, in accord with both the stochastic and silver models. Given that most blocks rest with the short axis vertical, fracture across the *L* or *M* axes is consistent with known fracture mechanics, whereby the centre of an object is the location, under loading, of the maximum in the tensile stress and the consequent nucleation point for fracture (Hiramatsu & Oka, 1966; Shipway & Hutchings, 1993). From this point, a fracture line develops to the block edges (Man *et al.,* 2018) transverse to the direction of tensile loading. For low values of static or dynamic loading, the rock eventually ruptures into two parts (Man *et al*., 2018). Thus, although a block on occasion might fracture across an axis at variance with the two models above, there is a tendency for blocks to evolve towards one or the other model. The system state attractors for these two models are shown in Fig. 7, wherein natural block shapes are considered. Importantly, compression and tensile fracture leads

in both models initially to uniquely defined anisotropic forms, although isotropic forms ($L = M = S$) can occur in principle with progressive fracture if the fracture rule in each model is relaxed and varied.

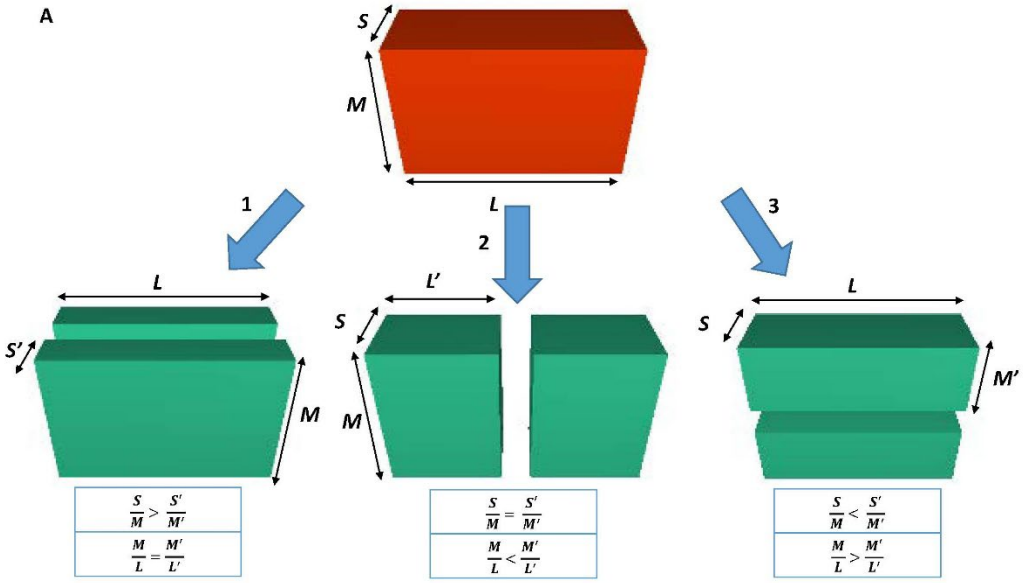

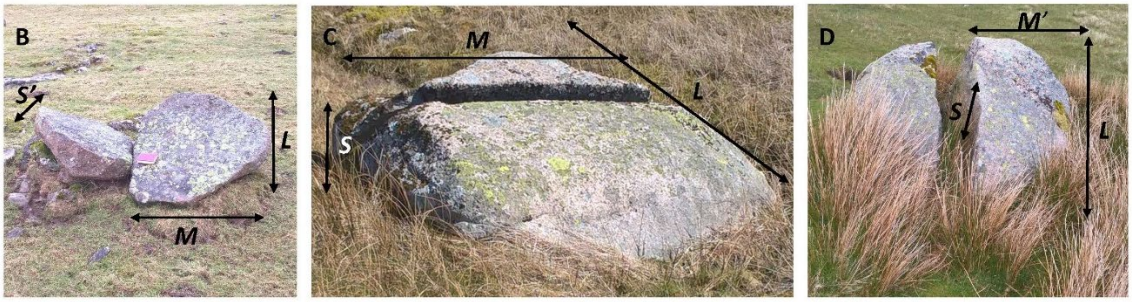

Figure 5: A) Schematic representation of the concept of the stochastic fracture model applied to a three-dimensional cuboid (enclosing an ellipsoid – see Fig. S1) subject to successive fracture given an assumed identical stress loading to the granite block at each fracture event. Fracture planes are orthogonal to a side and separate two pieces of equal mass. Shape self-similarity is not maintained upon successive fracture events. Three different fracture styles are possible within the model, as labelled 1, 2 and 3; B) Example of a well-rounded block split along a fracture plane consistent with model 1; C) Example of a well-rounded block split along a fracture plane consistent with model 2; D) Example of a well-rounded block split along a fracture plane consistent with model 3. The long axes are foreshortened in panels B, C and D.

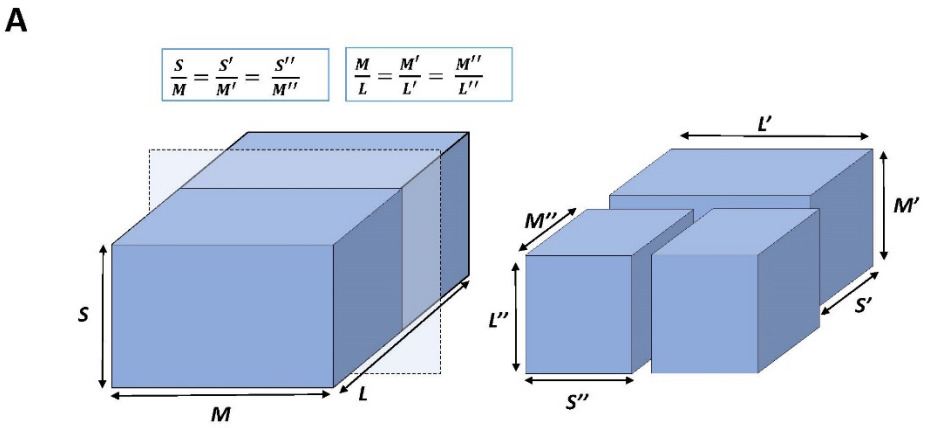

312

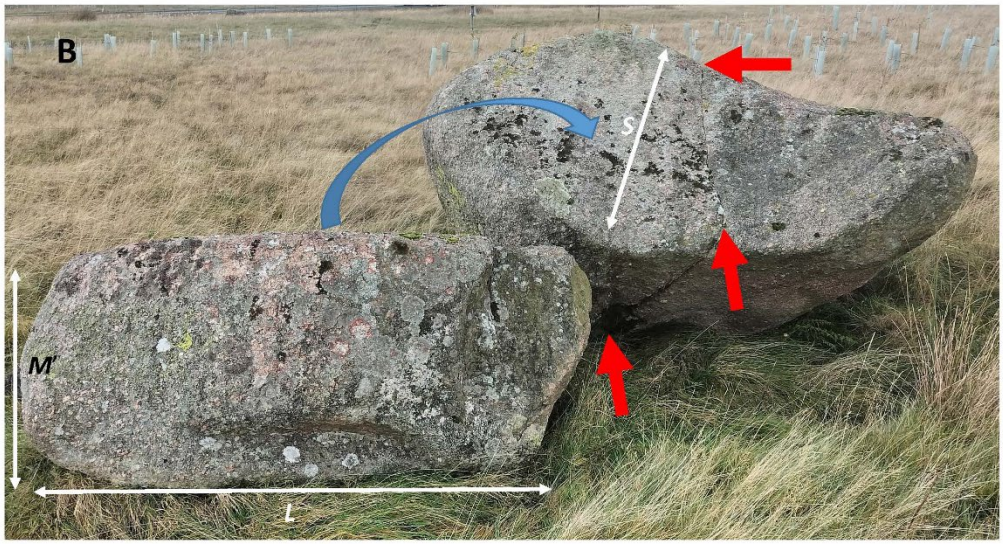

313

314 *Figure 6: A) Schematic representation of the concept of the silver ratio model applied to a three-*
315 *dimensional cuboid (– see Fig. S1) subject to successive fracture given an assumed identical direction*
316 *of stress loading to the granite block at each fracture event. Fracture planes are orthogonal to the*
317 *current long axis. Shape self-similarity is more closely maintained (in contrast to Fig. 5) upon successive*
318 *fracture events; B) Example of silver ratio block. Block to left is approximately the same size as the*
319 *block to the right and the lower surface (not seen) was originally on the top surface of the right-hand*
320 *block with the exposed failure plane bisecting the M-axis alignment of the original parent block. The*
321 *red arrows delineate a fracture plane, aligned with the M-axis of the right-hand block, which divides*
322 *the right-hand block into two near-equal halves.*

323

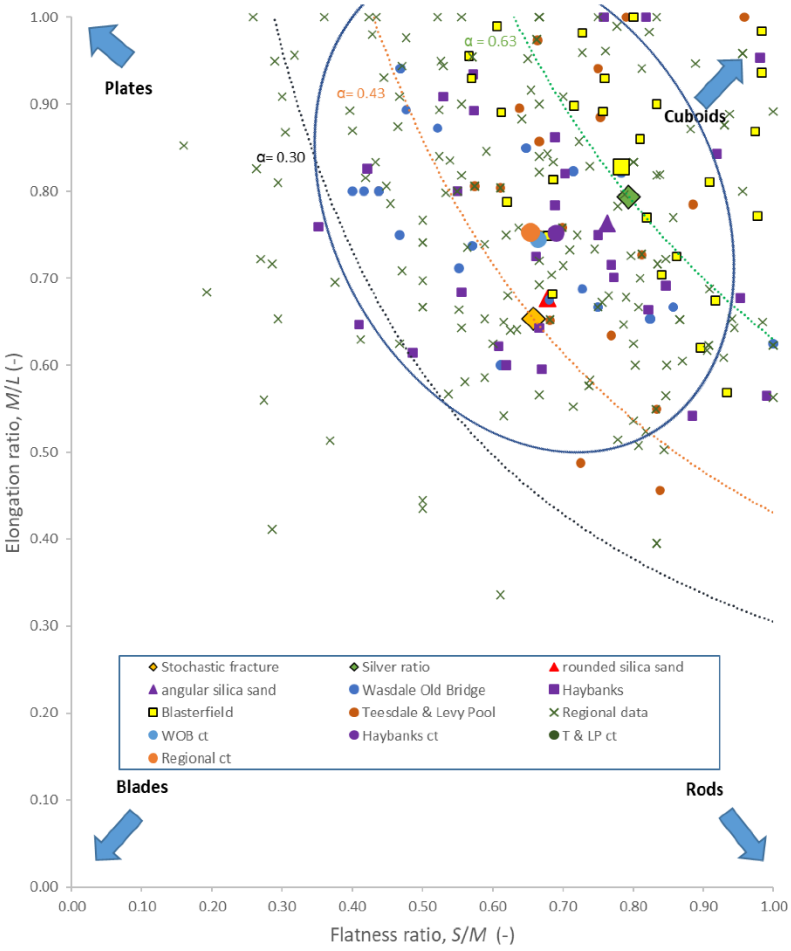

Figure 7: The shape relationship for blocks in terms of the Zingg (1935) ratios. The system state attractors for stochastic fracture (gold diamond) and silver ratio (green diamond) are shown, as are the central tendency shapes for mechanically crushed silica sand grains that were initial sub-rounded or angular (Seo et al., 2021). Curves represent the trend in values of M/L and S/M for constant values of S/L. ct symbols represent the central tendency of each population. Oval is the 95% contour after Oakey et al., 2005.

Within Fig. 7, the Zingg ratios (*S*/*M and M*/*L*) for the sampled locations are plotted together with a data set for the broader region (Regional data). Within Fig. 7, completely equant (isotropic) forms are absent and plate-like forms survive more readily than rods. Nonetheless, the central tendency of block shape within the regional data is *S*/*M* = 0.65 and *M*/*L* = 0.75; *i.e.*, roughly midway between the system state attractor for stochastic fracture and the silver ratio attractor. Lines of constant equal aspect ratios (*S*/*L*) are shown for the silver ratio model (α = 0.63) and for the stochastic fracture model (α = 0.43). Seo *et al*. (2021) showed that for homogeneous silica grains, fracture depended on initial

particle form (Fig. 7) with angular grains tending towards the silver ratio whilst rounded grains tended towards stochastic fracture. If the fracture process is scale-invariant, then the size differences between silica grains and the Shap blocks can be ignored, and one would expect the Shap granite (a largely homogeneous lithology) to migrate across the diagram from silver to stochastic fracture as cubic blocks become progressively more rounded and ellipsoidal. Blocks deviating from either model (either too long or flat, *e.g.*, approaching $\alpha = 0.30$), will tend to fracture and migrate back towards $\alpha = 0.43$, as is especially evident in Fig. S6B. The central tendencies of the regional data and each of the sampled locations are closely grouped between the central tendencies of the silver and stochastic fracture. The exception is the Blasterfield location which lies closer to the silver ratio, but with increased distance of transport, Teesdale & Levy Pool blocks are in accord with stochastic fracture. Thus, it is evident that block fracture fluctuates between each model, with a trend for constant equal aspect ratios close to $\alpha = 0.50$ (not plotted in Fig. 7).

Although Fig. 7 provides an impression of the spread of block shapes around a central tendency there is no clear impression of the actual shape evolution as possible representative shapes can only be selected arbitrarily from the data clouds. Further, only the cube (or sphere) limit point (*e.g.*, 1, 1 in Fig. 7) is real. Limit points for rods and plates exist only through mathematical definition, because as the rod and plate limit points are approached, rods become infinitely long and plates infinitely thin. Thus, representative shapes need to be selected objectively. To solve this problem the procedure of Oakey *et al*. (2005) was utilized to define representative shapes that define the 95% contour around the central tendency of the regional data, represented by the blue oval in Fig. 7. With reference to the position of the 95% contour in the blade quadrant, curve $\alpha = 0.30$ is selected to demarcate a lower bound for common block ratios; with a few plate-like or rod-like blocks occurring in the lower portion of the diagram.

3.3 Size evolution

The size distribution of the Shap granite blocks with distance from the pluton source has not received detailed attention, although Carling *et al*. (2013) provide some general observations suggesting there is size reduction with distance. In this study, the sample sizes were insufficient to demonstrate the reduction in block size expected with distance from the source outcrop. However, controls on size reduction are evident. Specifically, blocks greater than L = 4m are rare (Carling *et al*., 2013), the size being controlled by the close joint spacing of the granite at source (Firman, 1953). With few exceptions, large blocks (L > 3.0 m) do not occur beyond 7 km from the pluton, at which point medium blocks (2.5 > L > 1.5 m) become scarce, with small blocks (1.5 > L > 0.5 m) and cobble-sized material dominating with further dispersal (Carling *et al*., 2013). These observations indicate that there was a control on the upper size of blocks entrained from the pluton and fracture rapidly reduced block size inducing a crude size-reduction down plume within just a few kilometres. This process was accompanied by local deposition of abrasion and spallation debris as components of a subglacial traction till till. Nevertheless, the fracture mechanics that control block shape inevitably control size evolution (Figs. 5 and 6). For example, fracturing a parent cube with 4m long edges and its progeny across the L-axis, only six sequent fracture divisions are required to produce a 1 m cube, as will be demonstrated in the Discussion.

4 Discussion: The context of size and shape constraints

The initial hypothesis proposed that Sg ice-transported blocks would display changes in edge-rounding and shape with distance to the east from the pluton. As shown in the Results and elaborated below edge-rounding does change with distance but block shape is conservative.

Space-time substitution is an underlying tenant of this study, in that the size and shape characteristics of multiple individual blocks (an erratic plume), dispersing across the landscape, can reflect the

389 evolution of a single erratic block through time along the same general spatial trajectory. An adequate
390 number of sampled blocks are required for this analogy to hold because perturbations to the
391 population of erratics can occur during dispersal. For example, blocks can have been introduced to
392 the W-E trajectory of the study plume by N-S ice movements reworking blocks previously deposited
393 outside of the eastern-directed plume during periods of time after the main W-E ice flow. Also, for
394 the purposes of determining transport distance, a zero *x*-axis origin has been assumed to be the most
395 easterly outcrop of the pluton at Wasdale Crag. However, some blocks might have been sourced up
396 to a few kilometres to the west of Wasdale Crag. Despite these potential perturbations, which include
397 a small degree of subaerial weathering, the small sample sizes are sufficient to clearly demonstrate
398 systematic change in edge rounding due to ice transport as well as block shape evolution. Finally,
399 edge-rounding and shape are re-set to a degree for the children each time a parent block fractures,
400 so the process of rounding and shape adjustment is not a smooth function of distance from the
401 outcrop, as is explained below.
402
403 **4.1 A conceptual model of block edge rounding controls**
404
405 It should be acknowledged that this study has not considered abrasion of the faces of blocks but has
406 focussed on the edges which tend to abrade and round more rapidly than the associated faces
407 (Boulton, 1974). The edges of blocks still within the outcrop are sharp, albeit some are subject to a
408 slight degree of rounding in place (Fig. 4) from glacial wear, as well as a little post-glacial subaerial
409 weathering. Detached blocks close to the outcrop also tend to exhibit slightly ice-rounded edges, with
410 sharply angled joint planes characterising the other faces due to fracture release of the block from
411 outcrop. The increase in edge rounding with distance confirms the initial hypothesis.
412
413 Block edge rounding initially is constrained by the hardness of the Shap granite and the way it fractures
414 when first entrained at outcrop. The absence of significant edge rounding at the outcrop indicates

that blocks were entrained continually until the imposed stresses fell below that required to quarry further blocks. Otherwise, edge rounding of entrained blocks is associated with basal traction transport (Boulton, 1978; Hallet, 1979). Although the compressive strength of granite is high, the tensile strength is an order of magnitude lower; possible as low as 4% of the compressive strength, *i.e.,* 8 MPa (Anikoh *et al*., 2015; Demirdag *et al*., 2018; Engineering ToolBox, 2008; Yu *et al*., 2018). Thus, where compression is translated into flexure, the propensity of the block to elongate across the axis of flexure leads readily to fracture of the brittle granite. This condition means that many blocks close to source initially exhibited near right-angle edges (Fig. 4). Given this geometric constraint, radii of edge curvature inevitable are small initially, approaching the limit: $r_c = l/2$ and $r_c = h$, and increase with distance from the outcrop due to abrasion. However, fracture away from the outcrop introduces new sharp edges (Figs. 4 & 7), such that larger radii characterizing an individual edge-rounded block just before fracture are augmented by smaller radii. This change is reflected in the scatter of radii values found with increased distance from the outcrop (Fig. 4). However, as block size reduces, a condition is approached whereby the population of blocks are increasingly those which resist fracturing (see section 'Block size controls) which should allow edge rounding to become more persistent and thus more pronounced with distance. This condition may be approached in the case of the examples from Teesdale (Fig. 4A) where it is evident that short chords become fewer with distance as larger values of r_c begin to dominate the population. As blocks in transport can reorientate within the ice flow, edge rounding has no effect on block shape, given the shape definition herein. However, if blocks are not free to reorientate, a case not considered herein, the form of blocks can be significantly affected by abrasion in place (Boulton 1974; Hallet, 1979).

Although a positive exponential function (Equation 2) describes the increase in the mean edge rounding with distance from the source outcrop (Fig. 4A inset panel), the function must eventually transition to a negative function as abraded smaller blocks inevitably are characterized by smaller radii of curvature. This latter condition was not recorded within the current study and sampling at greater

441 distances from the source would be required to determine if this transition occurs. A block (*e.g.*, 1 m
442 cube) subject to edge rounding equally on all 12 edges, as per Equation 2, would have lost about 4%
443 of its mass after 10 km and 9% after 40 km so, in contrast, fracture into two self-similar parts whereby
444 50% of mass is lost, is more significant than edge-rounding in terms of mass loss per block. The greater
445 significance of fracture is consistent with studies of ice erosion by quarrying versus abrasion of basal
446 bedrock surfaces (see references in Cohen *et al*., 2006).
447
448 Rounding of individual bocks is not a steady process, as is evident from the data scatter in Fig. 4 and
449 is further illustrated in the following section. The process whereby the percentage of edges of
450 different generations are rounding with distance, or time, is shown schematically in Fig 8A, wherein
451 there are initially no more than 12 slightly rounded edges to a cube block newly released from outcrop
452 (see Supplementary Information for detail of the model). The model is simple but demonstrates the
453 complexity in edge rounding that must accompany successive fracturing of blocks. Fracturing the
454 block successively across the *L*-axis introduces new generations of fracture edges (sequent fractures
455 – Fig. 8B) at the same time as reducing the number of edges on each new block related to earlier
456 fracture events (see Supplementary Information for further detail). As the number of progeny blocks
457 increases exponentially for each fracture event (Fig. 8C), and each sibling can be further dissected
458 along one, two or three *M*-axes depending on block shape, a diagram including all fracture progeny
459 introduces unreasonable complexity, obscuring the key details. In Fig. 8A&B, for clarity, only one block
460 is followed through one to six sequent fractures, which reduces the number of data points for plotting
461 to a manageable number. The key point to illustrate is that the initial 'parent' block must be fractured
462 five times for one of the ensuing progenies to have lost all the initial 12 edges of the 'parent'. The
463 total number of initial parent edges is relatively persistent because there are 12 edges to begin with
464 (Fig. 8). Contrarily, only four new edges (Fig. 8A) per block are produced on each fracture event. Thus,
465 in contrast to the curve for the initial parent edges, the 1st fracture edges can be lost in as little as four
466 fracture events depending on which sibling block is considered. The 2nd fracture edges are lost by a

total of five fracture events and so on, as more fractures occur adding new fracture edges. Relaxing the model to allow fracture across either the *M* or *S* axis (see Supplementary Information) only adds one or two fracture events to the process of edge extinctions. Thus, by introducing new edges at each fracture event, rounding of the block with distance or time is not a steady progression, with well-rounded edges being lost as blocks are split at the same time as new immature edges are added to a population of sub-mature edges. The model may not apply beyond some undetermined number of fracture events if there is a critical minimum block size that is less susceptible to fracture (as was noted above) and rounding then can become pronounced. Nonetheless, this model explains the presence of a 'continuum' from well-rounded edges to less-well-rounded edges on many individual blocks. The issue as to whether there is a minimum block size is considered in the next section.

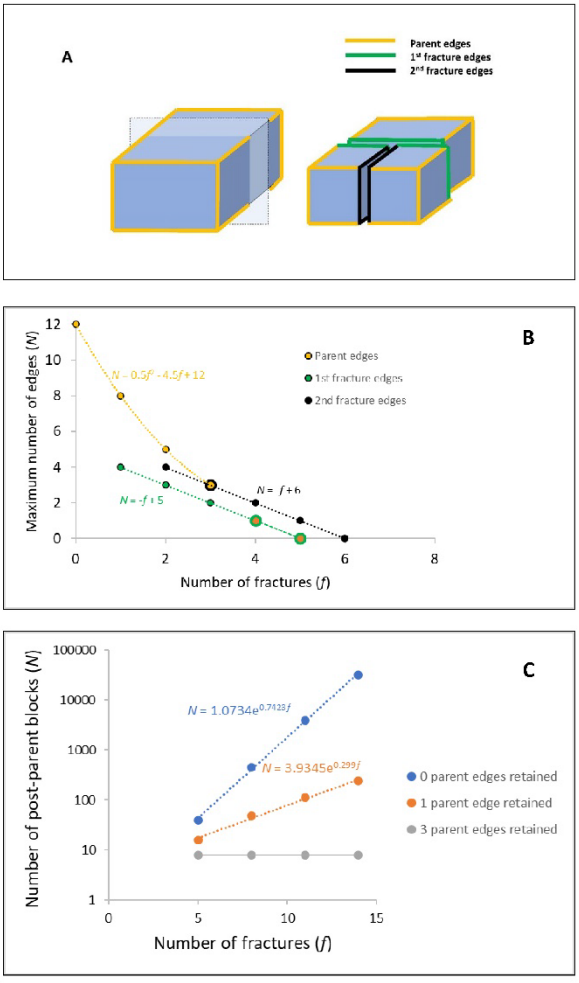

Figure 8: A) A regular block released from outcrop has 12 initial edges (Parent edges) all equally rounded. Fracturing the block at right angles introduces four new edges (1st fracture edges) to each of two sibling blocks, which edges are younger than the initial edges. A further fracture across the L-axis is indicated by 2nd fracture edges; B) The maximum number of edges of each generation on a block as a function of the number of fracture events, with only the parent edges and those edges related to the first two fracture events plotted; C) The total number of blocks created at each fracture event which retain 0, 1 or 3 of the original parent edges.

The significant mean edge rounding, with distance from outcrop (Fig. 4A inset panel), indicates that the blocks were transported within a mobile concentration of basal debris, in frequent block-to-block contact and in contact with the bedrock, leading to abrasion before being deposited within a subglacial traction till (Hallet, 1979). If the distance travelled towards the east and south is not the controlling factor, then the high degree of edge-rounding may be due to prolonged temporal transport, with some material moving east, south, and then north again, extending the transport distances. However, compatible with studies showing block modification after distances of only 0.4 km (Humlum, 1985; Lliboutry 1994; MacGregor *et al.* 2009), an alternative main explanation is preferred for the easterly edge-rounding trend. Although Sg is mechanically strong in compression (Goudie, 2006) it is susceptible to abrasion and tensile fracture for the following reason. The blocks contain large pink phenocrysts set within a matrix of smaller mineral crystals. The large pink crystals are orthoclase feldspar (Moh hardness 6 – 6.5). The other common minerals are glassy quartz (Moh hardness 7), white plagioclase feldspar (Moh hardness 6) and black biotite mica (Moh hardness 2.5 – 3) (Caunt, 1986). Thus, the granular composition of the granite with harder crystals adjacent to a soft mineral may aid rapid rounding by abrasion and facilitate tensile facture during glacial transport.

4.2 Block shape controls

Block shape is dependent on the initial controls exhibited at: 1) the outcrop of origin; and 2) the subsequent transport history.

1) The primary control is the intersection of sub-vertical joints (Firman, 1953) in the granite with horizontal expansion joint planes caused by unloading (Jahnes, 1943). Horizontal joints largely are due to glacio-isostatic rebound and surface erosion (Westaway, 2009), leading to the release of the residual stresses accumulated at depth (Berger & Pitcher, 1970). The resultant blocks initially tend to be cubic. Where blocks lie within a few metres from the parent outcrop, the block faces tend to be planar, although curved fractured surfaces occur occasionally, as do conchoidal fracture hollows on otherwise planar surfaces. Curved fracture surfaces tend to occur in homogeneous granite due to pressure unloading (Wang *et al*., 2022), which will have occurred as ice erosion reduced the overburden. Such joint-defined blocks within an outcrop are readily entrained by moving ice (Matthes, 1930; Morland & Boulton, 1975).

2) Although inhomogeneous blocks in traction may be envisaged as breaking down into multiple fragments at each compressive event (Boulton, 1978), the largely homogeneous nature of the Sg lithology leads to simple tensile fracturing, at each breakage event, whereby subsequent generations of blocks exhibit shapes largely similar to the parent forms. Thus, there is a tendency for equant blocks to persist, through time and distance, due to the tensile stresses associated with flexure across the stoss surfaces reducing block mass in accord with either the silver model or the stochastic model. This trend is indicated by the fact that stronger plate-like blocks occur less frequently away from the pluton in contrast to the general absence at distance of the weaker rod-like blocks. Thus, cuboids progress to form both cubes and cuboids such that the initial hypothesis is rejected.

4.3 Block size controls

Block size is dependent on the initial controls exhibited at: 1) the outcrop of origin; and 2) the subsequent transport history.

1) The primary control is the presence of the frequent, well-developed joint planes within the pluton (Firman, 1953; Caunt, 1986) which tend to define and delimit the range of the initial block sizes from *c*., 0.5 m to 4 m. Fault planes are of sufficient rarity to be ignored. Joints are largely orthogonal: *i.e*., sub-vertical and near horizontal but oblique joints also occur.

2) Once in ice-transport, other controls on block disintegration may pertain. In the present case, larger blocks close to the outcrop (< 0.8 km) often exhibit one (or more) intact or partially opened failure plane(s) inherited from the outcrop structure. More commonly, with distance from the outcrop (> 0.8 km), the planes of failure within individual blocks represent the directions of tensile and compressive forces exerted by the ice on the blocks (and thus bear no relationship to structure or composition), as appears to be the case where failure planes are aligned with the *L* or *M* axes. Fracture occurred when the effective tensile stress exceeded the yield strength of the blocks. Glacial unloading, and subsequent stress release, also may introduce planes of weakness within transported blocks. Adopting the stochastic fracture mode or the silver ratio model for block shape changes indicates that block volume effectively halves at each fracture event with consequent reduction in block size. This conclusion has implications for the fractal evolution of erratic size distributions which, for brevity, cannot be addressed within this paper.

Other small-scale planes of weakness can be attributed to spatial variations in the primary mineral composition (Grantham, 1928; Parsons & Lee, 2005) leading to textural and grain-size variations which can be visible rarely as parallel lineaments, and later hydrothermal alteration also induced compositional and hence structural variations (Caunt, 1986). These weaknesses lead to loss of small blocks and flakes from the larger parent blocks (see Supplementary Information) through spallation rather than fracture. Spallation may be related to the state of stress within a deforming till layer (LeBone Hooke & Iverson, 1995) rather than the tensile stress on the stoss side of a block which accounts for block fracture.

558

559 **4.4 General considerations**

560

561 A significant question is whether flowing ice can generate significant stress to fracture the granite
562 blocks. If the thickness of the deforming ice layer at the basal boundary is small relative to the size of
563 the boulder, then the compressive force is likely to dominate. However, if the converse applies then
564 the tensile force likely will dominate. Herein, given that there is no information as to the thickness of
565 the deforming layer, the distinction is not considered because, in most cases, blocks will fracture at a
566 lower stress due to tension in contrast to compression. In a consideration of similar situations,
567 emphasis was placed on the compressive strengths of blocks (Boulton, 1978) relative to the normal
568 stresses due to a static ice load above a block. In the present examples, the tensile strength of the
569 stoss side of a block resisting flexure is more relevant for brittle fracture and for granite can be as low
570 as 8 MPa, which is a tensile stress readily applied by a modest (*c.*, +100m thick) yet dynamic ice cover
571 (Hallet, 1996). The distribution of compressive and tensile forces over the stoss side of a block
572 adjacent to the bedrock at the base of an ice mass will be complex and variable through space and
573 time (Hallet, 1979; Morland & Boulton, 1975; Ficker *et al*., 1980; Cohen *et al*., 2005). Yet, a simple
574 example below outlines the principles within the context of Shap granite erratics. Although a more
575 complex and complete appreciation of the stress environment of a boulder would be preferred, a
576 simple force balance is utilized instead. Simplicity is dictated by the absence of data to inform a more
577 complex model.

578

579 Setting the tensile stress at failure to 8 MPa and treating the rectangular block as subject to a critical
580 average driving force (τ_c) (Benn & Evans, 2011, p.114) due to ice flow, transverse and longitudinal
581 shear stresses arise of equal magnitude. Setting the fracture focus at half the block width in the
582 direction of loading, neglecting any water pressure variations (Cohen *et al*, 2006) and deformation
583 within a basal till (LeBone Hooke & Iverson, 1995), and imposing the driving stress transverse to the

584 fracture plane, as little as 180 m thickness (*H*) of flowing glacial ice with an ice surface slope (α) of 1.5°
585 would be sufficient to induce fracture in the block:
586
587 $$\tau_c = \rho_i \, g \, H \, tan \, \alpha, \quad (3)$$
588
589 where ρ_i is the density of glacial ice and g is the acceleration due to gravity. The value of *H* = 180 m
590 pertains for a rectangular block with a surface area (*A*) defined by *L* = 2 m and *M* = 2 m (see
591 Supplementary Information for details). The effective instantaneous stress might be greater than as
592 given by Equation 3 (LeBone Hooke & Iverson, 1995) but for a block with *L* = 3 m, *M* = 1 m with the
593 long axis transverse to the ice flow the shear force maximum might be achieved with only 130 m of
594 ice cover (see Supplementary Information). To the east of the pluton the Last British Ice Sheet was
595 several hundred metres thick *c*., 25-22 ka BP (Evans *et al*., 2009), such that blocks would readily
596 fracture during full-glacial warm-based conditions where ice is flowing, as well as after the Late Glacial
597 Maximum when ice was thinning.
598
599 The smallest block sizes (*L* < *c*., 1.0 m) present in the field were not considered, which means that the
600 sampled population was truncated at the finer end. Nevertheless, although in some rock-types, a
601 lower limit to block strength may be related to a minimum structural block size (Dreimanis & Vagners,
602 1971; Lim *et al*., 2004; Domokos *et al*., 2015) this is unlikely to pertain to granite which breaks-down
603 to grus at the scale of the phenocrysts. None-the-less, fracture and surface wear, to an initial block
604 population, tend to result in the observed block population consisting of those blocks which are
605 strongly resistant to further comminution (Moss, 1972; Tavares and King, 1998; Larson & Mooers,
606 2004; Pfeiffer *et al*., 2022) which, in principle, enables some blocks to survive transport adjacent to
607 the sole of the ice for great distances before being deposited during the waning phase of the easterly
608 directed ice stream (Hallet, 1979). Thus, although there may be no lower effective block size, a
609 statistical increase in resistance to fracture of the block population with distance is likely evident as

610 witnessed by the increased rounding seen in the Teesdale population. The occasional far-travelled
611 large block, as noted in the Introduction, might be explained as being a statistically stronger example,
612 in contrast to the remainder of the population. Alternatively, large blocks can be cushioned within
613 the till body by smaller particles (Einav, 2007) thus avoiding fracture, or they can be transported
614 englacially, rather than basally, and consequently not subject to protracted abrasion and significant
615 compression whilst in traction. However, englacial blocks are more likely to be angular (Shilts, 1976;
616 Boulton, 1978) and might retain rugose faces.
617
618 Thus, although the reduction in plume parameters values, such as block size and concentration, are
619 commonly viewed as exponential functions of distance from the source (Shilts, 1976), such models
620 (*e.g.*, Fig. 4A inset panel) consider the sampled population as a whole and the inferences derived may
621 not apply to the transport history of individual blocks. Certainly, the reduction in edge rounding for
622 individual blocks is irregular with distance.
623
624 **5 Conclusions**
625
626 The hypothesis that granite blocks would display an increase in edge rounding with distance from the
627 source outcrop is confirmed, whilst the hypothesis that shape would evolve with distance is refuted.
628 Although the mean value for edge rounding for the whole block population increases exponentially
629 with distance, edge rounding on individual blocks is an irregular function mediated by block fracture
630 mechanics, as block size reduces (with shapes fluctuating between cuboids, slabs and rods) with
631 distance and new sharp edges are provided to partially edge-rounded blocks. Thus, edge rounding,
632 and shape coevolve as block size is reduced. Fracture transverse to block orientation is in accord with
633 the application of tensile stress which controls the process by which block form is conserved as block
634 size is reduced. Consideration of the orientation of the tensile fractures on blocks in the field might
635 be used to approximate the direction of ice flow at the time of fracture.

Overall, the results indicate that edge rounding is unlikely to be advanced if blocks continue to fracture. Well-rounded blocks must represent blocks that have resisted splitting. In the case of exceptionally large, rounded blocks, the rock mass likely is unusually homogeneous, lacking potential fracture lines. However, smaller blocks are less likely to contain potential fracture lines and so fracture should become less prevalent as blocks reduce in size, which then promotes edge rounding.

Future work should consider developing mathematical models that represent the function of edge rounding as predicated by a model (*e.g.*, silver ratio) describing block size reduction. Similar studies considering other lithologies (*e.g.*, stratified sedimentary rocks) likely would find different shape evolution patterns in contrast to the cuboid central tendency displayed by the homogeneous granite, with concomitant implications for edge rounding trends with time and distance.

Author contribution

PAC designed the study and conducted the field work, analysis, interpretation and drafting.

Competing interests

The author declares that he has no conflict of interest.

Acknowledgements

Emma Armstrong (Armstrongs Group) for access to the Shap (Pink) Quarry. Leslie Knight and David Evans (Durham University) provided information on the location of Shap granite erratics in Teesdale

and near Levy Pool. Leslie Knight provided the base image for Fig. 3A. Two anonymous referees are thanked for their commentaries which led to improved presentation of the final results.

Data Availability

Basic data are available upon reasonable request from the author.

References

Anikoh, G.A., Adesida, P.A., Afolabi, O.C.: Investigation of physical and mechanical properties of selected rock types in Kogi State using hardness tests. *Journal of Mining World Express*, 4, 37-51. DOI:10.14355/mwe.2015.04.004, 2015.

Benn, D.I. :The genesis and significance of 'Hummocky Moraine': Evidence form the Isle of Skye, Scotland. *Quaternary Science Reviews*, 11, 781-799. https://doi.org/10.1016/0277-3791(92)90083-K, 1992.

Benn, D.I., Evans, D.J.A.: Glaciers and Glaciation, Hodder, London. 802pp, https://doi.org/10.1111/j.1502-3885.2011.00212.x, 2011.

Berger, A.R., Pitcher, W.S.: Structures in granitic rocks: A commentary and a critique on granite tectonics. *Proceedings of the Geological Association of London*, 81, 441–461. https://doi.org/10.1016/S0016-7878(70)80006-2, 1970.

Bouchard, M.A., Salonen, V.-P.: Block transport in shield areas, Glacial Indicator Trains, Kujansuu, R., Saarnisto, M., (editors), Balkema, Rotterdam, 87-107, ISBN 9781003079415, 1990.

Boulton, G.S.: Processes and patterns of glacial erosion. Glacial Geomorphology, Coates, D. R., editor), Binghamton, N.Y., State University of New York, 41-87, Publications in Geomorphology, ISBN: 9789401164931, 1974.

Boulton, G.S.: Boulder shapes and grain-size distributions of debris as indicators of transport paths through a glacier and till genesis. *Sedimentology*, 25, 773-799. https://doi.org/10.1111/J.1365-3091.1978.TB00329.X, 1978.

British Standard Institution: Code of Practice for Site Investigations, BS 5930 HMSO, London, 1981.

Buscarnera, G., Einav, I.: The mechanics of brittle granular materials with coevolving grain size and shape. *Proceedings of the Royal Society*, A, 477: 20201005. https://doi.org/10.1098/rspa.2020.1005, 2021.

Carling, P.A., Su, T., Meshkova, L.: Distribution of Devensian glacial erratics and related evidence elucidate complex ice flow changes across a former ice divide: Northern England. *Proceedings of the Geologists' Association*, 134, 139-165. https://doi.org/10.1016/j.pgeola.2023.01.002, 2013.

Caunt, S.L.: Igneous and Metamorphic Processes in the Shap Granite and its Aureole. Unpubl. PhD thesis, University of Leeds, 337pp, https://etheses.whiterose.ac.uk/522/, 1986.

Clark, P.U., Dyke, A.S., Shakun, J.D., Carlson, A.E., Clark, J., Wohlfarth, B., Mitrovica, J.X., Hostetler, S.W., McCabe, M.: The Last Glacial Maximum. *Science*, 325, 710-714. https://doi.org/10.1126/science.1172873, 2009.

Cohen, D., Iverson, N.R., Hooyer, T.S., Fischer, U.H., Jackson, M., Moore, P.L.: Debris-bed friction of hard-bedded glaciers. *Journal of Geophysical Research*, 110, doi:10.1029/2004JF000228, 2005.

Cohen, D., Hooyer, T.S., Iverson, N.R., Thomason, J.F., Jackson, M.: Role of transient water pressure in quarrying: A subglacial experiment using acoustic emissions. J*ournal of Geophysical Research*, 111, F03006, doi:10.1029/2005JF000439, 2006.

Conroy, R.M., The RCSI Sample size handbook. Technical report, doi: 10.13140/RG.2.2.30497.51043 2018.

Daniel, W.W., Biostatistics: A Foundation for Analysis in the Health Sciences, 7th. New York, John Wiley & Sons, 1999.

Day, M. J. and Goudie, A. S.: Field assessment of rock hardness using the Schmidt test hammer. *BGRG Technical Bulletin*, 18, 19-29. 1977.

Demirdag, S., Sengun, N., Ugur, I., Altindag, R.: Estimating the uniaxial compressive strength of rocks with Schmidt rebound hardness by considering the sample size. *Arabian Journal of Geosciences*, 11, 502, https://doi.org/10.1007/s12517-018-3847-1, 2018.

Domokos, G, Kun, F, Sipos, A.A., Szabó, T.: Universality of fragment shapes. *Scientific Reports,* 5, 9147. doi:10.1038/srep09147, 2015.

Dreimanis, A., Vagners, U.J.: Bimodal distributions of rock and mineral fragments in basal tills. Till: A Symposium, Goldthwait, R.P. (Editor), Ohio State University Press, Columbus, 237-250, ISBN 9780814201480 1971.

Einav, I.:) Breakage mechanics -Part 1: Theory. *Journal of Mechanics and Physics of Solids*, 55, 1274-1297. https://doi.org/10.1016/j.jmps.2006.11.003, 2007.

Engineering ToolBox: *Compression and Tension Strength of some Common Materials*. [online] Available at: https://www.engineeringtoolbox.com/compression-tension-strength-d_1352.html, 2008 [Accessed 02 01 2023].

Evans, D.J.A.: Glacial erratics and till dispersal indicators. Encyclopaedia of Quaternary Science, S.A. Elias (Editor), Elsevier, Oxford, 975-978, ISBN 978-0-444-52747-9, 2007.

Evans, D.J.A., Livingstone, S.J., Vieli, A., O´ Cofaigh, C.: The palaeoglaciology of the central sector of the British and Irish Ice Sheet: reconciling glacial geomorphology and preliminary ice sheet modelling. *Quaternary Science Reviews*, 28, 739-757. doi:10.1016/j.quascirev.2008.05.011, 2009.

Evans, D.J.A., Phillips, E.R., Hiemstra, J.F., Auton, C.: Subglacial till: Formation, sedimentary characteristics and classification. *Earth-Science Reviews*, 78, 115-176, doi:10.1016/j.earscirev.2006.04.001, 2006.

Firman, R. J.: Metamorphism and Metasomatism around the Shap and Eskdale granites, Durham theses, Durham University. http://etheses.dur.ac.uk/9565/, 1953.

Ficker, F., Sonntag, G., Weber, E.: Asätze zur mechanischen deurung der rissentstehung bei parablrissen und sichelbrűchen auf glaziageformten felsoberflächen. *Zeitshcrift fűr Gletscherkunde und Glazialgeologie,* 16, 25-43, 1980.

Glasser, N.F.; Roman, M.; Holt, T.O.; Žebre, M.; Patton, H.; Hubbard, A.L.: Modification of bedrock surfaces by glacial abrasion and quarrying: Evidence from North Wales. *Geomorphology*, 365, 107283. https://doi.org/10.1016/j.geomorph.2020.107283, 2020.

Goudie, A.S.: The Schmidt Hammer in geomorphological research. *Progress in Physical Geography*, 30, 703-718. https://doi.org/10.1177/0309133306071954, 2006.

Grantham, D.R.: The petrology of the Shap Granite. *Proceedings of the Geological Association*, 39, 299-331. https://doi.org/10.1016/S0016-7878(28)80015-0, 1928.

Haldorsen, S.: Grain-size distribution of subglacial till and its relation to glacial crushing and abrasion. *Boreas*, 10, 91-105. https://doi.org/10.1111/j.1502-3885.1981.tb00472.x, 1981.

Hallet, B.: A theoretical model of glacial abrasion. Journal of Glaciology, 23, 39-50. https://doi.org/10.3189/S0022143000029725, 1979.

Hallet, B.: Glacial abrasion and sliding: Their dependence on the debris concentration in basal ice. *Annals of Glaciology*, 2, 23–28. https://doi.org/10.3189/172756481794352487, 1981.

Hallet, B.: Glacial quarrying: a simple theoretical model. *Annals of Glaciology*, 22, 1-8. https://doi.org/10.3189/1996AoG22-1-1-8, 1996.

Hiramatsu Y, Oka Y.: Determination of the tensile strength of rock by a compression test of an irregular test piece. *International Journal of Rock Mechanics and Mining Sciences & Geomechanic Abstracts,* 3, 89–90. doi:10.1016/0148-9062(66)90002-7, 1966.

Hodgson, E.: The granite drift of Furness. *Geological Magazine*, 7, 328-339. https://doi.org/10.1017/S0016756800209801, 1870.

Holland, E.G.: Shap Granite. *Mine & Quarry Engineering*, 25, 2-15, 1959.

Hopkins, W.: On the transport of erratic blocks. *Transactions of the Cambridge Philosophical Society*, 8, 220-240, 1849.

Humlum, O.: Changes in texture and fabric of particles in glacial traction with distance from source, Myrdalsjokull, Iceland. *Journal of Glaciology,* 31 (108), 150-156. https://doi.org/10.3189/S0022143000006390, 1985.

Jahns, R. H.: Sheet structure in granites, its origin and use as a measure of glacial erosion in New England. *Journal of Geology*, 51, 71– 98, 1943.

Kirkbride, M.P.: Boulder edge-roundness as an indicator of relative age: A Lochnagar case study, *Scottish Geographical Journal*, 121, 219-236, https: doi: 10.1080/00369220518737232, 1985.

Kujansuu, R., Saarnisto, M.: Glacial Indicator Tracing, Balkema, Rotterdam, 252pp, ISBN 9781003079415, 1990.

Larson, P. C. & Mooers, H. D.: Glacial indicator dispersal processes: a conceptual model. *Boreas*, 33, 238–249. DOI 10.1080/03009480410001262, 2004.

Le Bone Hooke, R., Iverson, N.R.: Grain-size distribution in deforming subglacial tills: Role of grain fracture. *Geology*, 23, 57-60. https://doi.org/10.1130/0091-7613(1995)023%3C0057:GSDIDS%3E2.3.CO;2, 1995.

Li, X.F., Li, H.B., Zhang, Q.B., Jiang, J.L., Zhao, J.: Dynamic fragmentation of rock material: Characteristic size, fragment distribution and pulverization law. *Engineering Fracture Mechanics*, 199, 739-759. https://doi.org/10.1016/j.engfracmech.2018.06.024, 2018.

Lim, W.L., McDowell, G.R., Collop, A.C.: The application of Weibull statistics to the strength of railway ballast. *Granular Matter*, 6, 229–237. http://dx.doi.org/10.1007/s10035-004-0180-z, 2004.

Lliboutry, L.L.: Monolithologic erosion of hard beds by temperate glaciers. *Journal of Glaciology*, 40, 433-450. https://doi.org/10.3189/S0022143000012314, 1994.

Livingstone, S.J., Evans, D.J.A., Ó Cofaigh, C., Davies, B.J., Merritt, J.W., Huddart, D., Mitchell, W.A., Roberts, D.H., Yorke, L.: Glaciodynamics of the central sector of the last British-Irish Ice Sheet in Northern England. *Earth-Science Reviews*, 111, 25-55. https://doi.org/10.1016/j.earscirev.2011.12.006, 2012.

MacGregor, K., Anderson, R.S., Waddington, E.D.: Numerical modeling of glacial erosion and headwall processes in alpine valleys. *Geomorphology*, 103, 189–204. https://doi.org/10.1016/j.geomorph.2008.04.022, 2009.

Man, K., Wang, K., Liu, X.: Dynamic tensile properties of granite varied with depths under a similar loading rate. *Advances in Civil Engineering*, Article ID 6048312, https://doi.org/10.1155/2018/6048312, 2018.

Matthes, F. E.: Geological history of the Yosemite Valley. U.S. Geological Survey. Professional Paper 160, 160pp, 1930.

Merritt, J.W., Hall, A.M., Gordon, J.E., Connel, E.R.: Late Pleistocene sediments, landforms and events in Scotland: a review of the terrestrial stratigraphic record. *Earth and Environmental Science Transactions of the Royal Society of Edinburgh*, 110, 39-91. https://doi.org/10.1017/S1755691018000890, 2019.

Morland, L.W., Boulton, G.S.: Stress in an elastic hump: the effects of glacier flow over elastic bedrock. *Proceedings of the Royal Society*, *A,* 344, 157-173. https://doi.org/10.1098/rspa.1975.0096, 1975.

Moss, A.J.: Technique for assessment of blocks breakage in natural and artificial environments. *Journal of Sedimentary Petrology*, 42, 725–728. https://doi.org/10.1306/74D7261C-2B21-11D7-8648000102C1865D, 1972.

Nicholson, H.A.: On the granite of Shap, in Westmoreland. *Transactions of the Edinburgh Geological Society,* 1, 133-37, https://doi.org/10.1144/transed.1.2.133, 1868.

Oakey, R.J., Green, M., Carling, P.A., Lee, M.W.E., Sear, D.A., Warburton, J.: Grain-shape analysis– A new method for determining representative blocks shapes for populations of natural grains. *Journal of Sedimentary Research*, 75, 1065-1073. https://doi.org/10.2110/jsr.2005.079, 2005.

Olsen, L.: A method for determining total block roundness in sediments. *Boreas*, 12, 17-21. http://dx.doi.org/10.1111/j.1502-3885.1983.tb00355.x, 1983.

Pfeiffer, A. M., Morey, S., Karlsson, H. M., Fordham, E. M., & Montgomery, D. R.: Survival of the strong and dense: Field evidence for rapid, transport-dependent bed material abrasion of heterogeneous source lithology. *Journal of Geophysical Research: Earth Surface*, 127, e2021JF006455. https://doi.org/10.1029/2021JF006455, 2022.

Parsons I., Lee, M.R.: Minerals are not just chemical compounds. *The Canadian Mineralogist*, 43, 1959-1992. https://doi.org/10.2113/gscanmin.43.6.1959, 2005.

Seo, D., Sohn, C., Cil, M.B., Buscarnera, G.: Evolution of blocks morphology and mode of fracture during the oedometric compression of sand. *Géotechnique*, 71, 853-865. https://doi.org/10.1680/jgeot.18.P.300, 2021.

Shilts, W.W.: Glacial till and mineral exploration. Glacial Till, An Interdisciplinary Study, R.F. Legget (editor), Royal Society of Canada, Special Publication, 12, 205-224, https://doi.org/10.2136/sssaj1977.03615995004100010004x, 1976.

Shipway P, Hutchings I.: Fracture of brittle spheres under compression and impact loading. I. Elastic stress distributions. *Philosophical Magazine, A* **67**, 1389–1404. https://doi.org/10.1080/01418619308225362, 1993.

Tavares, L.M., King, R.P.: Single-blocks fracture under impact loading. *International Journal of Mineral Processing*, 54, 1–28. https://doi.org/10.1016/S0301-7516(98)00005-2, 1998.

Ugelvig, S. V., Egholm, D.L., Iverson, N.R.: Glacial landscape evolution by subglacial quarrying: A multiscale computational approach. *Journal of Geophysical Research: Earth Surface*, 121, doi:10.1002/2016JF003960, 2016.

Wager, L.R.: A stage in the decomposition of biotite from the Shap Granite. *Proceedings of the Yorkshire Geological Society*, 25, 366-342, 1944.

Wang, X.-Y., Yin, Y.-C., Xing, M.-L., Zhang, D.-D., Chen, Y., Wang, E.-C.: Microsimulation study on energy release and rock block ejection force of granite under different unloading conditions. *Frontiers in Earth Science*, 10:909371. doi: 10.3389/feart.2022.909371, 2022.

Wentworth, C.K.: A method of measuring and plotting the shapes of pebbles. *US Geological Society Bulletin* 730-C, 91-102. doi: 10.3133/B730C, 1923.

Westaway, R.: Quaternary uplift of northern England. *Global and Planetary Change*, 68, 357-382. https://doi.org/10.1016/j.gloplacha.2009.03.005, 2009.

Yu, M., Wei, C., Niu, L., Li, S., Yu, Y.: Calculation for tensile strength and fracture toughness of granite with three kinds of grain sizes using three-point-bending test. *PLoS ONE*, 13, e0180880. https://doi.org/10.1371/journal. pone.0180880, 2018.

Zingg, T.: Beitrag zur schotteranalyse. PhD thesis, ETH Zurich. https://www.reasher-collection.ethz.ch/handle/20.500.11850/135183, 1935.